Science and Technology Indonesia
e-ISSN:2580-4391 *p*-ISSN:2580-4405
Vol. 9, No. 4, October 2024

Research Paper

Corn-Cob-Waste-Based $Fe_{2.75}Mn_{0.25}O_4$/rGO Nanocomposite Application as Anti-Radar Coatings

Lalu Saefullah[1,3]*, Kormil Saputra[1,4], Wida Puteri Agista[2], Masruroh[1], Dionysius J. D. H. Santjojo[1], Istiroyah[1]

[1]*Department of Physics, Universitas Brawijaya, Malang, Jawa Timur, 65145, Indonesia*
[2]*Department of Physics, Universitas Negeri Malang, Malang, Jawa Timur, 65145, Indonesia*
[3]*Military Weapons Engineering Technology Study Program, Poltekad Kodiklatad Malang, Kota Batu, Jawa Timur, 65324, Indonesia*
[4]*Physics Study Program, Universitas Mataram, Mataram, Nusa Tenggara Barat, 83115, Indonesia*
***Corresponding author**: lalusaeful@student.ub.ac.id

Abstract
Radar-absorbent materials (RAMs) have become essential technologies in fields that require them, such as the military. Their working principle is that they absorb electromagnetic waves and prevent their reflection. In developing the manufacturing of RAMs, high-performance materials are needed for effective use as RAMs. In general, RAMs possess two essential properties: magnetic and dielectric. This research reports the author's successful synthesis of an $Fe_{2.75}Mn_{0.25}O_4$/rGO nanocomposite as an anti-radar material using the coprecipitation method. Interestingly, the main precursors used were natural materials, namely iron sand and corn cob waste. XRD, FTIR, and SEM-EDX characterized the research samples to determine the nanocomposite's structure and phase, functional groups, and morphology after doping. XRD characterization results showed that $Fe_{2.75}Mn_{0.25}O_4$/rGO nanoparticles had a cubic crystal structure and that there were no new peaks, which indicates that Mn had been successfully substituted into Fe. FTIR test results showed that the $Fe_{2.75}Mn_{0.25}O_4$/rGO nanocomposite had Mn and Fe−O functional groups in octahedral and tetrahedral positions at wave numbers of 418–480 cm^{-1} and that there were C=C functional groups at the wave number of 1629 cm^{-1}. SEM results showed that the nanocomposite comprised $Fe_{2.75}Mn_{0.25}O_4$ particles in agglomerated spheres and corn-cob-based rGO in sheet form, with a grain size of around 26–31 nm. EDX test results showed the appearance of Fe, Mn, O, and C elements. It was also found that the 3-mm-thick $Fe_{2.75}Mn_{0.25}O_4$/rGO nanocomposite sample achieved the highest reflection loss (RL) value of -43.6 dB at a frequency of 8.5 GHz, indicating a significant radar wave absorption capability.

Keywords
Manganese, $Fe_{2.75}Mn_{0.25}O_4$, rGO, Nanocomposite, Corn Cobs

Received: 26 March 2024, Accepted: 24 June 2024
https://doi.org/10.26554/sti.2024.9.4.798-805

1. INTRODUCTION

Nanotechnology is experiencing rapid development (Aziz et al., 2019), and it is especially true when it comes down to nanomaterials. Nanomaterials are nano-sized chemical compounds with various functions, including antibacterial (Ghosh et al., 2019), waste absorbent (Ghosh et al., 2019), and anti-radar functions (Handoko et al., 2019). Anti-radar technology is a wave-absorbing technology that can detect the position of an object specifically with the help of radio waves (Subagio et al., 2020). The mechanism by which an object is detected using radar is based on the geometric angle of the specific wave beam reflection at the receiver (Izhar Friswara et al., 2021). As such, it is deemed increasingly important to explore essential topics related to anti-radar nanomaterials, including the topic of radar-absorbent materials (RAMs) (Kholil et al., 2022).

Nanomaterials for RAM applications take many forms, including nanomagnetic and dielectric materials, which work together in cohesion to absorb waves optimally (Kholil et al., 2022; Puteri Agista et al., 2023). Nanomagnetic materials must be conductive, making it easier to absorb electrical sources. The most widely researched nanomagnetic material is magnetite (Fe_3O_4), doped with various materials such as Mn, Zn, and Co to form composites with various materials such as carbon nanotubes (CNT), zinc oxide (ZnO), and titanium oxide (TiO_2). However, none of these materials have generated optimum results to be applied as RAMs (Ali et al., 2020; Chang et al., 2021). These materials are often considered inappropriate, with numerous drawbacks including active site clumping and low reflection loss, which are the main concerns in this research field. This leads to a need for an alternative advanced material that can be used for RAM applications, such as rGO, as proven

by various research reports.

Reduced graphene oxide, or rGO, has the advantage of undergoing optical modulation in response to light, which enables adaptive regulation against radar waves (Askari et al., 2022). In addition, rGO has a low density and can reduce the aggregation of $Fe_{2.75}Mn_{0.25}O_4$, making it suitable for use as an anti-radar material (Saputra et al., 2021). This material has hydroxyl and carboxyl structure defects that support the absorption of radar waves through the principle of surface polarization (Puteri Agista et al., 2023). In recent decades, rGO has been explored in various fields such as electrochemical capacitors (Manjunatha et al., 2020), pollutant adsorbents and removal of rhodamine B (RhB) dye from water (Elbasuney et al., 2020), photocatalysts, and the manufacture of organic photovoltaics (Brankov et al., 2020). In related research, rGO has been shown to increase the effective reflection loss. However, reports on rGO nanocomposites as RAMs have been rare.

Our previous report on Fe_3O_4-rGO (RFO) as an efficient RAM has been verified using various characterization tools (Askari et al., 2022; Elbasuney et al., 2020). The critical role of Fe_3O_4 in the RFO nanocomposite is to provide apparent support in improving the mechanical strength and uniform dispersibility of RFO. In addition, the properties of Fe_3O_4 are compatible with rGO, which helps improve the reflection loss. Therefore, we look to conduct research with $Fe_{2.75}Mn_{0.25}O_4$ composited with corn-cob-based rGO. Corn cob is an underutilized waste with 39.80% elemental carbon content and 30.91% hemicellulose content (An et al., 2022). Corn cob use is expected to improve our previous research, in addition to the fact that using a natural material such as corn cob gives an added value in line with the zero-waste principle.

2. EXPERIMENTAL SECTION

2.1 Materials

The materials used in this study included natural iron sand that had been separated from Sine Beach in Tulungaggung, Indonesia, $MnCl_3$ (Merck, Germany), corn cobs from Pasar Besar, Malang City, Indonesia, HCl (12 M, 99.9%, Merck), $MnCl_2.6H_2O$ (Merck), NH_4OH (6.5 M, 99.9%, Merck), deionized water (Nurra Gemilang, Indonesia), distilled water (Nurra Gemilang, Indonesia), 96% ethanol (Merck, Indonesia), paint (Agatha Paint, Indonesia), and steel plates (3 mm and 4 mm thick, Grade A type AH36).

2.2 Characterization

The $Fe_{2.75}Mn_{0.25}O_4$/rGO nanocomposite was characterized to determine its structure, crystal size, phase, and lattice parameters using X-ray Diffraction (XRD) Spectroscopy (X'Pert Pro, Cu-Kα 1.540 Å). A Fourier-transform infrared (FTIR) spectrophotometer (Shimadzu, IRPrestige21 type) was utilized to determine the Fe_3O_4/rGO functional group. The test was conducted at the Central Laboratory of the Faculty of Mathematics and Natural Sciences, State University of Malang. Furthermore, to identify the samples morphology, particle size, and elemental composition, Scanning Electron Microscopy-Energy Dispersive X-ray (SEM-EDX) (FEI brand, Inspect-S50 type) was used. The samples magnetic properties were tested using a vibrating-sample magnetometer (VSM) (OXFORD VSMl.2H). Simultaneously, the reflection loss of the samples was tested to determine the samples absorption performance using a vector network analyzer (VNA) (RS ZVA67).

2.3 Preparation of rGO Nanocomposite Samples

Synthesis of rGO was conducted using the thermal reduction method, with a prefix of burning dried corn cobs to obtain charcoal. The corn cob charcoal was crushed and sieved to obtain fine powder. Next, the corn cob charcoal powder was carbonated at 400°C for three hours in a furnace. The corn cob charcoal powder was weighed 5 g and mixed with 50 mL of distilled water. This mixture was put into an ultrasonic cleaner for two hours to be homogenized. The sample was centrifuged at 6000 rpm for 20 minutes to form a precipitate. The precipitate was filtered and dried at 100°C until rGO powder was obtained.

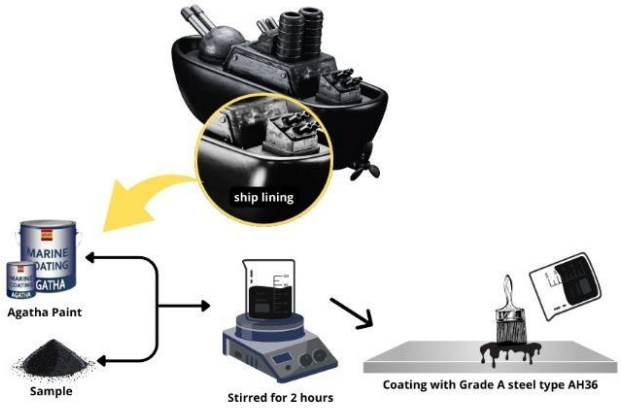

Figure 1. $Fe_{2.75}Mn_{0.25}O_4$/rGO Nanocomposite Powder Coating on Grade A Steel Plates

2.4 Preparation of $Fe_{2.75}Mn_{0.25}O_4$/rGO Nanocomposite Samples

Iron sand, taken from Sine Beach, Tulungagung, was dried in the sun until dry and then separated using a permanent magnet from a mixture of other compounds to form pure iron sand. The separated iron sand was then reacted with HCl to obtain an $FeCl_3$ solution, which was filtered using filter paper. Then, Mn was added to form $Fe_{2.75}Mn_{0.25}O_4$ by stirring a mixture of the filtered solution and $MnCl_2.6H_2O$. The obtained $Fe_{2.75}Mn_{0.25}O_4$ was then synthesized with 1 gram of rGO. After that, 19 mL of NH4OH was added until a black precipitate formed with a pH value of 7. The black precipitate was filtered/extracted using a permanent magnet. The synthesis result was then washed using distilled water and ethanol un-

til reaching neutral pH. $Fe_{2.75}Mn_{0.25}O_4$/rGO nanocomposite powder was obtained after heating at 100°C for 2 hours.

2.5 Coating of $Fe_{2.75}Mn_{0.25}O_4$/rGO on Steel Plates

Agatha paint and $Fe_{2.75}Mn_{0.25}O_4$/rGO was mixed in a ratio of 1:1 with a stirring speed of 750 rpm at room temperature for two hours until homogeneous. Then, the mixture was coated on 3-mm- and 4-mm-thick AH36-type steel plates. The coating was left to dry at room temperature. An illustration of the coating is presented in Figure 1.

3. RESULTS AND DISCUSSION

3.1 $Fe_{2.75}Mn_{0.25}O_4$/rGO XRD Results

The X-ray diffraction pattern identification results of the corn-cob-based rGO and the $Fe_{2.75}Mn_{0.25}O_4$/rGO nanocomposite with Mn doping are shown in Figure 2. The X-ray diffraction pattern of rGO from corn cobs, as shown in Figure 2, shows an amorphous peak at an angle of 2θ = 20–25°. A peak in that range indicates the detection of rGO. This is confirmed by Puteri Agista et al. (2023), according to whom rGO from corn cobs is indicated by a peak in the angle range of 2θ = 15–30°, as determined by the structure of an aromatic layer graphite (002) arrangement. This phase belongs to the carbon-graphite type with a hexagonal crystal system and a group spacing of R-3m (Mojtahedi et al., 2020). A similar peak was also confirmed by Rani et al. (2020), who stated that a peak at 2θ = 25.9° indicates rGO. The weak peak of rGO was undetectable because more $Fe_{2.75}Mn_{0.25}O_4$ nanoparticles were formed, which covered the base plane of rGO (Sunaryono et al., 2019; Zhang et al., 2020).

Figure 2 also shows the X-ray diffraction pattern of $Fe_{2.75}Mn_{0.25}O_4$/rGO nanoparticles. Based on the figure, diffraction peaks were detected at around 2θ = 30°, 35.4°, 43.2°, 53.6°, 57.6°, and 62.7°. Analysis results showed that these detected peaks correspond to Miller indices (220), (311), (400), (422), (511), and (440), respectively. However, there should be a small peak in the range of 20–28° with the Miller index (002), as shown in Figure 2, which indicates the detection of rGO. In addition, it was observed that no new peaks arose in the X-ray diffraction pattern, indicating that no new phases emerged following the inclusion of Mn in Fe_3O_4. Ardiyanti et al. (2023) stated that the absence of new peaks in $Fe_{2.75}Mn_{0.25}O_4$ indicates that Mn^{2+} has successfully entered into Fe^{3+} instead of manganese oxide deposits on the Fe_3O_4 surface.

The figure also shows that the Mn doping of the nanocomposite could be seen if the diffraction peak shifted towards a lower 2θ than the Fe_3O_4 data. This shift was related to the more significant value of the lattice parameter. The increase in the lattice parameter was due to Mn^{2+} having a larger ionic radius (0.81 Å) than Fe^{3+} (0.77 Å) (Zhan et al., 2018). These results indicate that some Fe^{3+} ions in the tetrahedral structure were replaced by Mn^{2+} ions (Sunaryono et al., 2023).

This analysis was carried out by comparing the research data with the ICSD database number 30860, and it was found that the crystal structure was of the cubic spinel type. This finding is supported by Saputra et al. (2021), who discovered that the

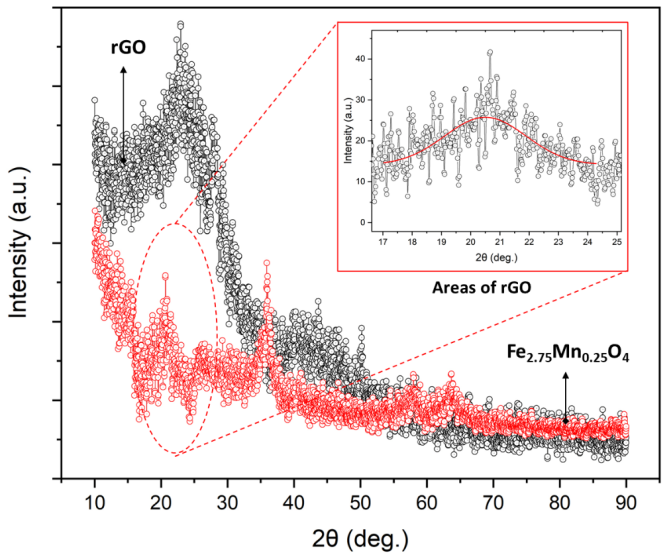

Figure 2. X-ray Diffraction Patterns of Corn-Cob-Based rGO and $Fe_{2.75}Mn_{0.25}O_4$/rGO

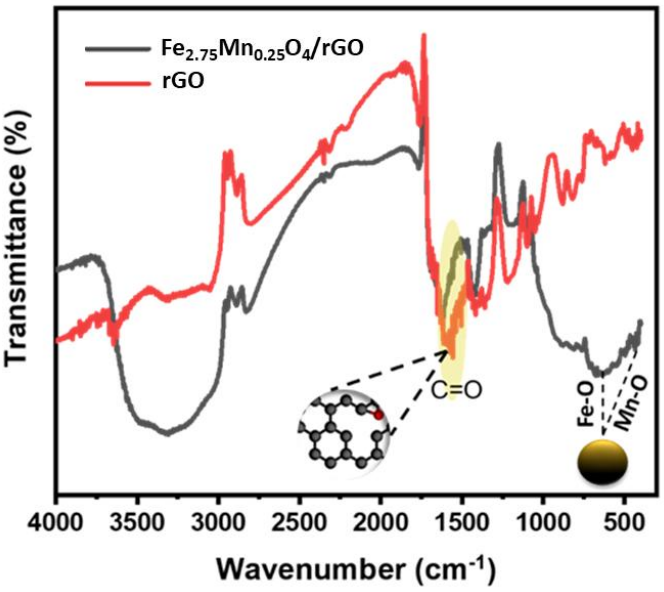

Figure 3. Functional Groups of rGO and $Fe_{2.75}Mn_{0.25}O_4$/rGO

nanocomposite crystal structure follows Fe_3O_4 in the form of cubic spinel. This finding is also supported by the analysis results in Table 1, according to which the lattice parameter increased to 8.380 Åfrom $Fe_{2.75}Mn_{0.25}O_4$. In addition, the crystal size of the nanocomposite decreased after Mn doping. Meanwhile, in the tetragonal structure, the crystal size and Mn composition increased (Sunaryono et al., 2023).

This was influenced by the increasing pH, which would cause the crystal size to decrease, as explained by Zhang et al. (2020). The neutral pH obtained in this research reduced the RAM corrosion rate. Taufiq et al. (2015) synthesized

Table 1. Diffraction Data Analysis Results of the $Fe_{2.75}Mn_{0.25}O_4$/rGO nanocomposite

Sample	Crystal Size (nm)	Lattice Constant (a = b = c) (Å)	Volume (Å^3)	ρ(g.cm^{-3})
$Fe_{2.75}Mn_{0.25}O_4$/rGO	11.5	8.38	588.4	5.23

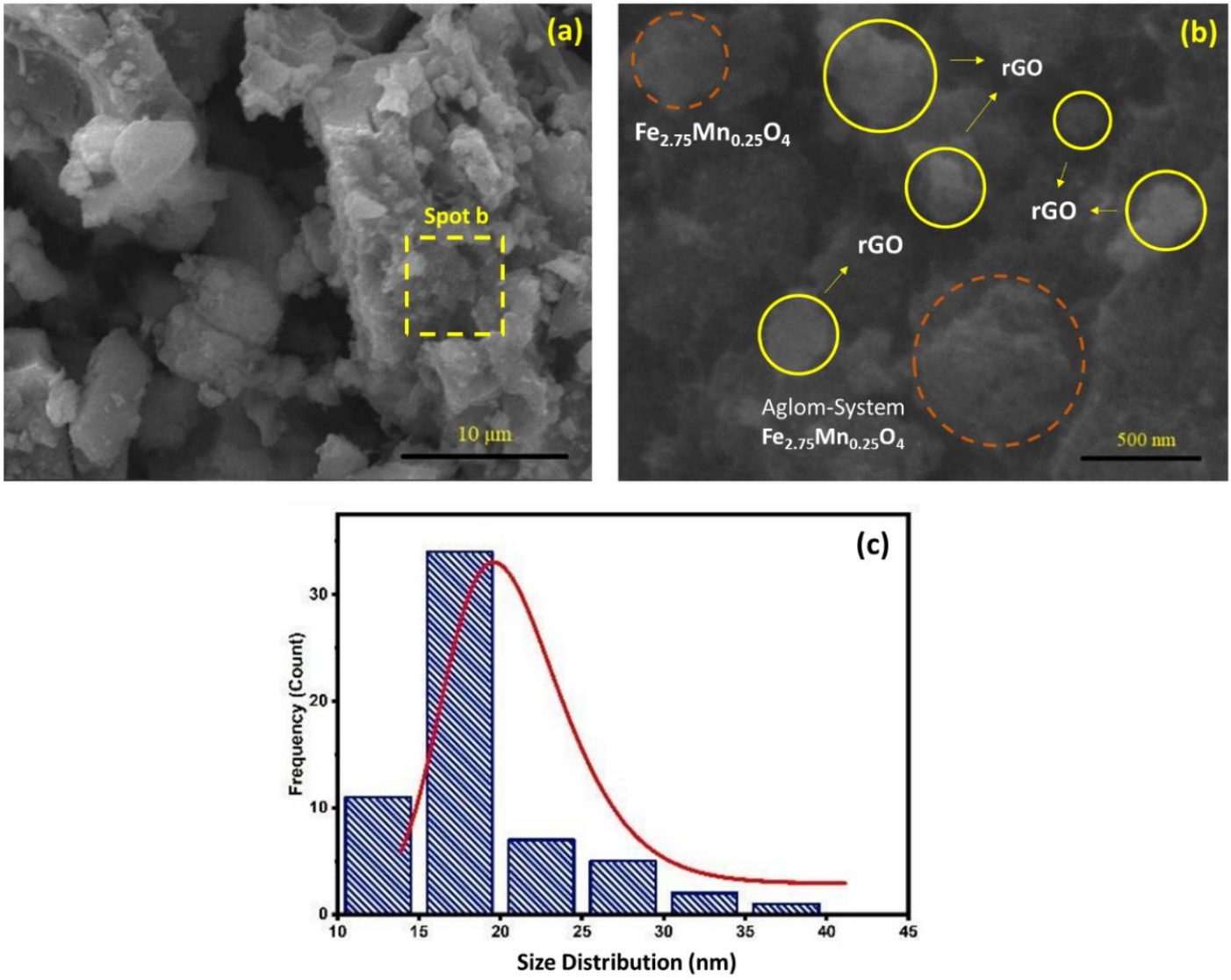

Figure 4. The Morphology and Surface Particle Size Distribution of the $Fe_{2.75}Mn_{0.25}O_4$/rGO Nanocomposite

$MnFe_2O_4$ using the coprecipitation method and found that doping x = 0.1, 0.3, and 0.5 had particle sizes of 10 nm, 12 nm, and 13 nm respectively. This study also obtained small sizes, which affected the composite's surface area. The smaller the particle size, the greater the parameter lattice and the larger the surface area.

3.2 Functional Groups of $Fe_{2.75}Mn_{0.25}O_4$/rGO and rGO

The FTIR characterization test results of the $Fe_{2.75}Mn_{0.25}O_4$/rGO nanocomposite with Mn doping can be seen in Figure 3.

Figure 3 illustrates the FTIR spectra of rGO and $Fe_{2.75}Mn_{0.25}O_4$/rGO in the 400–4000 cm^{-1} wave number range. In both samples, we could identify C=O functional groups at wave numbers of 1642–1516 cm^{-1}, indicating alkene groups and double bonds in the graphene structure, characteristic of reduced graphene (Amri et al., 2023). In addition, vibrations in the octahedral bond of Mn−O were visible at wave numbers of 418–480 cm^{-1}, and vibrations in the tetahedral bond of Fe−O were visible at the wave number of 700 cm^{-1} (Saputra et al., 2021).

Based on analysis results, in the rGO sample, C−O bonds were successfully identified in the wave number ranges of 1078–

1220 cm^{-1} and 2310–2346 cm^{-1} (Amri et al., 2023), while wave numbers of 1190 cm^{-1} and 1382 cm^{-1} are related to C−OH stretching vibrations, indicating the presence of hydroxyl groups after reduction (Hafeez et al., 2019; Rani et al., 2020). In addition, the nanocomposite showed a small band at 2918 cm^{-1} of C−H bond, which refers to the bond between a carbon atom in the reduced graphene structure with two hydrogen atoms (Ghosh et al., 2019). The stretching of the C=O and C−O bonds in the rGO sample indicates the possible presence of ketone groups (C=O) and hydroxyl groups (C−OH) in rGO. Although these bonds were generally reduced during the reduction process, they can still be seen in the FTIR spectra.

3.3 The Morphology and Particle Size Distribution of the $Fe_{2.75}Mn_{0.25}O_4$/rGO Nanocomposite

The SEM-EDX characterization test results on the $Fe_{2.75}Mn_{0.25}O_4$/rGO nanocomposite morphology are presented in Figure 4.

Figure 4 represents the surface morphology of the samples with a magnification of 10 μm to 500 nm. All samples had morphology with a distribution of large particle voids and spheres attached to the voids. Physically, the chunks of void particles represented the rGO material. In contrast, the small spheres attached to the large chunks represented $Fe_{2.75}Mn_{0.25}O_4$ particles synthesized from natural materials that tended to agglomerate, in this case corn cobs, which according to previous research appeared like porous chunks (Sunaryono et al., 2023). $Fe_{2.75}Mn_{0.25}O_4$ is like a sphere of particles that stick together, as was reported by Niranjana et al. (2023), who fabricated an Fe_3O_4/rGO composite material.

Furthermore, Figure 4c represents the particle size distribution of $Fe_{2.75}Mn_{0.25}O_4$/rGO doped with Mn. The particles had a particle size distribution of 15–20 nm. The particles were found to experience agglomeration, where they tended to gather in one place. Agglomeration was caused by the van der Waals force that appeared on the particles due to the large ratio of cross-sectional area to cross-sectional volume (Ahmadpour Kermani et al., 2021).

The size of these particles affects the surface area and mechanical properties of a RAM. Suppose the crystal and grain size grows smaller due to reduction. In that case, a considerable absorption value will be generated because the small particle size will increase the surface area and reduce the interference of electromagnetic wave absorption by magnetic and dielectric dipole moments in the RAM.

3.4 VSM Characterization for the $Fe_{2.75}Mn_{0.25}O_4$/rGO Sample

The VSM characterization results of the $Fe_{2.75}Mn_{0.25}O_4$/rGO nanocomposite are shown in Figure 5. The figure presents M−H hysteresis curves at room temperature.

Based on the VSM characterization results in Figure 5, a molar fraction of Mn = 0.25 indicates that the sample was superparamagnetic. This was due to the coercivity value of the sample, which was close to zero, and the particle size in

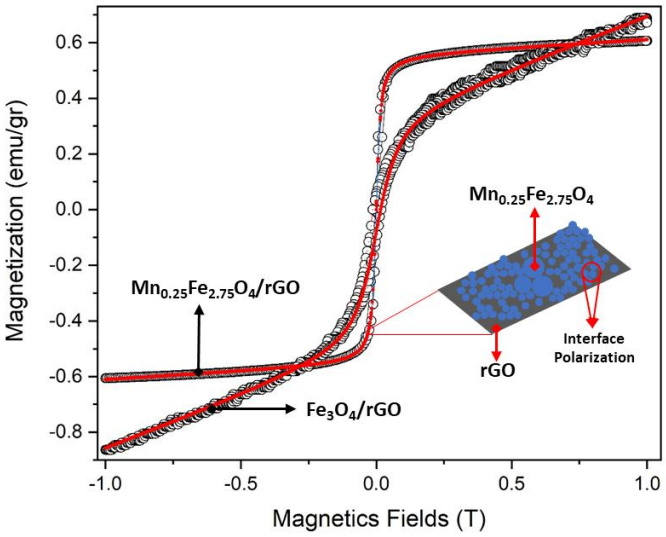

Figure 5. Hysteresis Curves for Fe_3O_4/rGO and $Fe_{2.75}Mn_{0.25}O_4$/rGO

nanometers (Sunaryono et al., 2019). The sample had a significant enough saturation magnetization value, where Mn_x = 0.25 had a saturation magnetization value of 32.83 emu/gram. Size and saturation magnetization are influenced by the size of the aggregation and fractal dimension. The hysteresis curves presented in Figure 5 were derived from fitting using the Langevin equation (Equation (1)) (Vroylandt, 2022).

$$M = Ms\left(coth\left(\frac{\mu H}{k_B T}\right) - \frac{k_B T}{\mu H}\right) \quad (1)$$

where M is magnetization, μ is the magnetic moment, H is the magnetic field (T), k_B is Boltzman's constant, which is 1.38×10^{-23} J/K, and T is room temperature (K). Using this equation, the values of several magnetic parameters, including saturation magnetization (Ms), remanent magnetization (Mr), and coercivity field (Hc), could be obtained. According to domain theory, the smaller the grain size and crystallinity, the fewer the plural domains. In a single domain, the number of magnetic dipole moments becomes more prominent, so the magnetic saturation value becomes bigger (Zhan et al., 2018). Mn doping will increase the dipole moment of the $Fe_{2.75}Mn_{0.25}O_4$ magnetic material, confirming that magnetization increases with Mn doping. This is consistent with the research results of Zhang et al. (2020), who reported an Ms value of Fe_3O_4 of 27.5 emu/g. Taufiq et al. (2015) reported an Ms value of fluid $Fe_{2.75}Mn_{0.25}O_4$ of 4.41 emu/g, which increased to 4.79 emu/g after doping with Mn.

In this study, the $Fe_{2.75}Mn_{0.25}O_4$/rGO nanocomposite had a greater saturation magnetization value than Fe_3O_4 alone, in which case the powder form of the sample exhibited a good effect. In addition, the characterization results using VSM confirmed that doping with Mn^{2+} ions with a concentration of Mnx = 0.25 in the $Fe_{2.75}Mn_{0.25}O_4$/rGO nanocomposite had

changed the sample's magnetic properties to soft magnetic.

Radar wave absorption can be identified through characterization testing using a vector network analyzer (VNA) (Kholil et al., 2022). In VNA testing, the data obtained are scattering parameters known as S-Parameters (Scattering Parameters). The S-Parameters reflect microwaves' reflection and transmission behavior at the VNA port. This information is essential for determining the reflection loss (RL) of materials to microwaves in the X-band frequency between 8 and 12 GHz. This range is the general working area for radar waves. RL measures how much a material can absorb waves. The higher the RL value, the greater the material's ability to absorb the microwaves. This means that a larger RL value indicates that the material is more effective at absorbing waves than materials with smaller RL values (Saravanan et al., 2023).

3.5 VNA Characterization Results for $Fe_{2.75}Mn_{0.25}O_4$/rGO Samples with Thickness Variations of 3 mm and 4 mm

The result of VNA characterization can be seen in Figure 6.

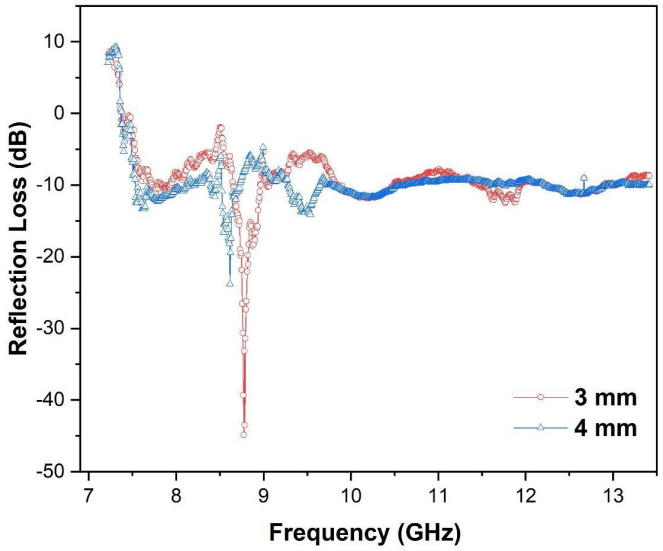

Figure 6. VNA Characterization Results of $Fe_{2.75}Mn_{0.25}O_4$ /rGO Samples with Thicknesses Variations of 3 and 4 mm

In this study, 3-mm- and 4-mm-thick $Fe_{2.75}Mn_{0.25}O_4$/rGO nanocomposite samples were used to evaluate radar wave absorption. The RL graph shows that the 3-mm-thick sample had a higher RL value than the 4-mm-thick sample. This indicates that the thickness of the sample affected the sample's wave absorption capability, in which case the 3 mm thickness was the most optimal of the two thickness variations. The explanation is that at a thickness of 3 mm, the material composition reached an optimal level of stability, allowing for more dipole-dipole rotations and magnetic dipole interactions at higher energies, resulting in more excellent wave absorption. These results align with previous research by Ding et al., who also found that a 3 mm thickness provides higher RL values than a 2 mm thickness (Gang et al., 2021; Saravanan et al., 2023). Specifically, the RL values for the 3 mm and 4 mm variations are presented in Table 2.

The test results at various thicknesses (3 mm and 4 mm) of the $Fe_{2.75}Mn_{0.25}O_4$/rGO nanocomposite samples showed that the largest reflection loss (RL) value was recorded at the thickness of 3 mm, reaching -43.6 dB at a frequency of 8.5 GHz. Analysis of the graph in Figure 6 showed that all nanocomposite samples exhibited a significant radar absorption capability. This indicates that adding the magnetic element Mn and incorporating it with an rGO dielectric material effectively enhances the wave absorption capability, which is relevant for reducing RAM applications. Similar findings were reported by Ding et al., who recorded RL values of -15.5 dB at 6.6 GHz for pure $Fe_{2.75}Mn_{0.25}O_4$ and -27.2 dB at 5.5 GHz for $Fe_{2.75}Mn_{0.25}O_4$/rGO nanocomposite. This confirms that Mn doping and incorporation with rGO can increase the absorption value. This can be explained by the resonance in the composite, which is different from RAM materials that only consist of magnetic or dielectric elements. $Fe_{2.75}Mn_{0.25}O_4$/rGO composite creates magnetic loss, dielectric loss, and polarization properties of the interface between $Fe_{2.75}Mn_{0.25}O_4$ and rGO.

The microwave absorption value is also affected by permeability, permittivity, and crystal size, as seen in the XRD results. Small crystal size, resulting from the reduction process, increases the absorption ability. This is because a large particle size reduces the surface area, interfering with the absorption of electromagnetic waves. This is consistent with the XRD results with a recorded particle size of about 11.5 nm. In addition, SEM analysis results in Figure 6 showed the morphology of the sample and the degree of porosity that affected energy dissipation. Porosity impeded the movement of spin waves in the samples, increasing energy dissipation in this material.

Table 2. RL Parameter Values and Frequencies of Samples by Thickness Variation

Thickness	RL value (dB)	Frequency (GHz)
3 mm	43.6	8.5
4 mm	28.9	8.3

4. CONCLUSIONS

A nanocomposite of $Fe_{2.75}Mn_{0.25}O_4$ and corn-cob-based rGO was successfully synthesized using the environmental coprecipitation method. $Fe_{2.75}Mn_{0.25}O_4$ was detected as crystals with a cubic structure and a relatively small crystal size of 11.5 nm. Meanwhile, the presence of rGO was confirmed by CC bonding at wave numbers of 418–480 cm^{-1}, associated with Mn−O octahedral bond vibrations. The intrinsic vibration of the Fe−O tetrahedral bond was found at a wave number of 700 cm^{-1}. The sample's morphology, based on SEM results, showed that rGO had a shape resembling chunks and $Fe_{2.75}Mn_{0.25}O_4$ took the form of spheres that spread and stuck to the rGO chunks. With the incorporation of Mn doping

and rGO composites, the RL values of samples with variations in thickness increased, although not significantly, because the nanocomposite consisted of magnetic loss and dielectric loss that increased the radar absorption. Interestingly, the RL value of the $Fe_{2.75}Mn_{0.25}O_4$/rGO nanocomposite produced was relatively high at a thickness of 3 mm, namely -43.6 dB, with a frequency of 8.5 GHz. An RL value > -20 dB indicates that the nanocomposite had a radar absorption capability of 96.9–99.0%.

5. ACKNOWLEDGMENT

We would like to sincerely thank Universitas Brawijaya and POLTEKAD Kodiklat TNI AD Malang for their invaluable support and provision of advanced laboratory facilities. The assistance and encouragement from the faculty and staff at both institutions were instrumental in completing this research.

REFERENCES

Ahmadpour Kermani, S., S. Salari, and P. Ghasemi Nejad Almani (2021). Comparison of Antifungal and Cytotoxicity Activities of Titanium Dioxide and Zinc Oxide Nanoparticles with Amphotericin B Against Different Candida Species: *In Vitro* Evaluation. *Journal of Clinical Laboratory Analysis*, **35**(1); e23577

Ali, G. W., O. W. Guirguis, M. Gobara, S. F. M. Mustafa, N. A. El-Zaher, and W. I. Abdel-Fattah (2020). On the Optical Characterization and Biological Implications of Titania Phases. *Optical Materials*, **109**; 110269

Amri, A., A. Lesbani, and R. Mohadi (2023). Malachite Green Dye Adsorption from Aqueous Solution Using a Ni/Al Layered Double Hydroxide-Graphene Oxide Composite Material. *Science and Technology Indonesia*, **8**(2); 280–287

An, Y., Q. Luo, Y. Zhong, X. Ma, S. Li, J. Wu, H. Na, Z. Sun, J. Zhu, and J. Chen (2022). The Green Design of Corncob Cellulose/Reduced Graphene Oxide-Derived Hierarchical Porous Aerogels for Efficient Dye Adsorption. *New Journal of Chemistry*, **46**(31); 15024–15031

Ardiyanti, A. D., S. Sunaryono, A. Choerullah, H. Wisodo, N. Mufti, and A. Taufiq (2023). Structure and Specific Absorption Rate Identification of $Mn_{0.25}Fe_{2.75}O_4/NiCo_2O_4$ Magnetic Nanocomposites. *Key Engineering Materials*, **941**; 165–172

Askari, M. B., P. Salarizadeh, H. Beitollahi, S. Tajik, A. Eshghi, and S. Azizi (2022). Electro-Oxidation of Hydrazine on $NiFe_2O_4$-rGO as a High-Performance Nano-Electrocatalyst in Alkaline Media. *Materials Chemistry and Physics*, **275**; 125313

Aziz, Z. A. A., H. Mohd-Nasir, A. Ahmad, S. H. Mohd. Setapar, W. L. Peng, S. C. Chuo, A. Khatoon, K. Umar, A. A. Yaqoob, and M. N. Mohamad Ibrahim (2019). Role of Nanotechnology for Design and Development of Cosmeceutical: Application in Makeup and Skin Care. *Frontiers in Chemistry*, **7**

Brankov, B., A. Stanojević, M. Nenković-Riznić, and M. Pucar (2020). The Possibilities for Implementation of Photovoltaic Solar Panels in Multi-Family Housing Areas. In *Proceedings of 8th International Conference on Renewable Electrical Power Sources*. pages 167–175

Chang, M., Z. Jia, S. He, J. Zhou, S. Zhang, M. Tian, B. Wang, and G. Wu (2021). Two-Dimensional Interface Engineering of $NiS/MoS_2/Ti_3C_2T_x$ Heterostructures for Promoting Electromagnetic Wave Absorption Capability. *Composites Part B: Engineering*, **225**; 109306

Elbasuney, S., G. S. El-Sayyad, M. Yehia, and S. K. Abdel Aal (2020). Facile Synthesis of RGO-Fe_2O_3 Nanocomposite: A Novel Catalyzing Agent for Composite Propellants. *Journal of Materials Science: Materials in Electronics*, **31**; 20805–20815

Gang, Q., M. Niaz Akhtar, and R. Boudaghi (2021). Development of High-Efficient Double Layer Microwave Absorber Based on Fe_3O_4/Carbon Fiber and Fe3O4/rGO. *Journal of Magnetism and Magnetic Materials*, **537**; 168181

Ghosh, S., S. Ganguly, P. Das, T. K. Das, M. Bose, N. K. Singha, A. K. Das, and N. C. Das (2019). Fabrication of Reduced Graphene Oxide/Silver Nanoparticles Decorated Conductive Cotton Fabric for High Performing Electromagnetic Interference Shielding and Antibacterial Application. *Fibers and Polymers*, **20**(6); 1161–1171

Hafeez, H. Y., S. K. Lakhera, M. Ashokkumar, and B. Neppolian (2019). Ultrasound Assisted Synthesis of Reduced Graphene Oxide (rGO) Supported $InVO_4$-TiO_2 Nanocomposite for Efficient Hydrogen Production. *Ultrasonics Sonochemistry*, **53**; 1–10

Handoko, E., I. Sugihartono, M. A. Marpaung, U. Cahyana, S. Aritonang, J. Zulkarnain, R. Rusmono, A. Taufiq, S. Sunaryono, and M. Randa (2019). Complex Permittivity, Permeability and Microwave Absorption Studies of Double Layer Magnetic Absorbers Based on $BaFe_{12}O_{19}$ and $BaFe_{10}CoZnO_{19}$. *Materials Science Forum*, **966**; 302–307

Izhar Friswara, A. C., K. Anwar, and L. O. Nur (2021). Multiple Frequencies Signal Absorber for Anti-Radar Applications in High Speed Flying Devices. In *2021 IEEE Symposium On Future Telecommunication Technologies (SOFTT)*. pages 12–16

Kholil, M. A., P. Priyono, and A. Subagio (2022). Multiwalled Carbon Nanotubes and Zinc Oxide Using a High Energy Milling Method for Radar-Absorbent. *Materials Research Express*, **9**(2); 025003

Manjunatha, C., V. Chirag, B. W. Shivaraj, N. Srinivasa, and S. Ashoka (2020). One Pot Green Synthesis of Novel rGO@ZnO Nanocomposite and Fabrication of Electrochemical Sensor for Ascorbic Acid Using Screen-Printed Electrode. *Journal of Nanostructures*, **10**(3); 531–539

Mojtahedi, S., M. Karimipour, E. Heydari-Bafrooei, and M. Molaei (2020). Application of Ascorbic Acid in the Synthesis of rGO/Micro-Octahedral Cu2O Nanocomposites and Its Effect on the Wide Linear Response Range of Glucose Detection. *Microchemical Journal*, **159**; 105405

Niranjana, J. S., H. Koyakutty, A. A. Thomas, and M. J. Bushiri (2023). Novel Synthesis of Multi-Layered rGO/ Fe_3O_4

Nanocomposite in a Single Step and Its Efficient Electrochemical Sensing of Vitamin C. *Materials Science and Engineering: B*, **290**; 116283

Puteri Agista, W., S. U. Intan Subadra, A. Taufiq, A. Hidayat, E. Handoko, M. Alaydrus, T. Amrillah, and I. Jeerapan (2023). Exploring the Role of Mn^{2+} in the Structure, Magnetic Properties, and Radar Absorption Performance of $Mn_xFe_{3-x}O_4$-DEA/MWCNT Nanocomposites. *RSC Advances*, **13**(42); 29332–29341

Rani, S., S. Kapoor, B. Sharma, S. Kumar, R. Malhotra, and N. Dilbaghi (2020). Fabrication of Zn-MOF@rGO Based Sensitive Nanosensor for the Real Time Monitoring of Hydrazine. *Journal of Alloys and Compounds*, **816**; 152509

Saputra, K., S. Sunaryono, S. Hidayat, H. Wisodo, and A. Taufiq (2021). Investigation of Nanostructural and Magnetic Properties of $Mn_{0.25}Fe_{2.75}O_4$/AC Nanoparticles. *Materials Today: Proceedings*, **44**; 3350–3354

Saravanan, A., P. Thirumurugan, S. Rajeshkannan, and S. Sridhar (2023). Effect of Corn Cob Carbon Quantum Dots and Areca Husk Microfiber on EMI Shielding Effectiveness of Flexible PVA Thin Film at 8–20GHz Frequency Bands. *Biomass Conversion and Biorefinery*; 1–8

Subagio, A., M. A. Kholil, W. Ristiawan, and P. Priyono (2020). Anti-Radar Application of Multiwalled Carbon Nanotubes and Zinc Oxide Synthesized Using a Hydrothermal Method. *Materials Research Express*, **7**(10); 105009

Sunaryono, S., N. M. Chusna, M. F. Hidayat, A. Choerullah, S. Hidayat, N. Mufti, A. Apriharta, A. N. Afandi, J. Rajagukguk, N. A. N. N. Malek, and A. Taufiq (2023). Investigating the Specific Absorption Rate and Antimicrobial Activity of $Mn_{0.25}Fe_{2.75}O_4$/Ag Ferrogel Based on Carboxymethyl Cellulose/Polyvinyl Alcohol Composite Polymer. *Journal of Thermoplastic Composite Materials*, **36**(12); 4905–4926

Sunaryono, S., K. Saputra, A. Hidayat, C. I. Yogihati, S. T. Wicaksono, N. Hidayat, S. Hidayat, and S. Soontaranon (2019). Magneto-Thermal Effect in $Mn_{0.25}Fe_{2.75}O_4$-PEG Nanoparticles and Their Potential as Hyperthermia Therapy. *IOP Conference Series: Materials Science and Engineering*, **515**(1); 012008

Taufiq, A., Sunaryono, E. G. Rachman Putra, A. Okazawa, I. Watanabe, N. Kojima, S. Pratapa, and Darminto (2015). Nanoscale Clustering and Magnetic Properties of $Mn_xFe_{3-x}O_4$ Particles Prepared from Natural Magnetite. *Journal of Superconductivity and Novel Magnetism*, **28**(9); 2855–2863

Vroylandt, H. (2022). On the Derivation of the Generalized Langevin Equation and the Fluctuation-Dissipation Theorem. *Europhysics Letters*, **140**(6); 62003

Zhan, Y., Y. Meng, W. Li, Z. Chen, N. Yan, Y. Li, and M. Teng (2018). Magnetic Recoverable $MnFe_2O_4$/Cellulose Nanocrystal Composites as an Efficient Catalyst for Decomposition of Methylene Blue. *Industrial Crops and Products*, **122**; 422–429

Zhang, M., F. Zhao, T. An, Y. Yang, H. Li, Q. Pan, X. Wang, and Z. Jiang (2020). Catalytic Effects of rGO–MFe_2O_4 (M= Ni, Co, and Zn) Nanocomposites on the Thermal Decomposition Performance and Mechanism of Energetic FOX-7. *The Journal of Physical Chemistry A*, **124**(9); 1673–1681

